Met. Mater. Int., Vol. 20, No. 1 (2014), pp. 41~47
doi: 10.1007/s12540-014-1010-4

Effect of Deformation Induced Transformation of ε-Martensite on Ductility Enhancement in a Fe-12 Mn Steel at Cryogenic Temperatures

Jung-Su Kim[1], Jong Bae Jeon[2], Joong Eun Jung[1], Kyung-Keun Um[3], and Young Won Chang[1,*]

[1]POSTECH, Department of Materials Science and Engineering, Pohang, Gyeongbuk 790-784, Korea
[2]Max-Planck-Institut für Eisenforschung, Max-Planck-Straße 1, 40237 Düsseldorf, Germany
[3]POSCO Research Laboratories, Pohang, Gyeongbuk 790-300, Korea

(received date: 10 July 2013 / accepted date: 11 July 2013)

Metastable ε-martensite (ε-Ms) formed during a prior heat treatment of Fe-12Mn steel has been reported to transform into α-Ms during subsequent inelastic deformation. This deformation induced phase transformation (DIPT) from ε-Ms to α-Ms has been investigated in the present study within the framework of kinetics relation proposed based upon an internal variable theory of inelastic deformation. The ε-Ms phase was found to become more stable at lower temperatures to provide more prolonged DIPT from ε-Ms to α-Ms during an inelastic deformation at cryogenic temperatures, contrary to the case of austenite phase in various *transformation induced plasticity* steels being more stable at higher temperatures. This reversed stability-temperature relationship in Fe-12Mn steel appeared to provide a significant ductility enhancement at lower temperatures as well as significant strengthening effect.

Key words: deformation induced phase transformation (DIPT), ε-martensite, α-martensite, transformation kinetics, stability, ductility

1. INTRODUCTION

Phase transformation from meta-stable austenite to martensite during plastic deformation has widely been studied for various austenitic steels including stainless steels, high nickel alloys, and high manganese steels [1-8]. Large ductility enhancement has been reported in these steels, christening them as '*transformation induced plasticity*' (TRIP) steels [9]. The ductility enhancement in these TRIP steels has generally been attributed to the suppression of necking due to increased work-hardening rate caused by transformed martensite phase during inelastic deformation [10-14]. This type of conventional approach cannot, however, provide a plausible explanation in regard to what causes this TRIP phenomenon. The terminology TRIP appears to be, in fact, coined from the observation of enhanced elongation accompanying martensitic transformation, without concerning what has induced martensitic transformation.

An entirely different new approach has therefore been proposed by one of the authors utilizing the concept of an internal variable theory for inelastic deformation based directly on well-known dislocation dynamics [15]. This internal variable theory regards inelastic deformation as a natural process to reduce an internal strain energy accumulated in the form of glide dislocations within crystalline materials during inelastic deformation. Another way to effectively relieve this stored internal strain energy could be through phase transformation, which might naturally be called then as a new terminology of '*deformation induced phase transformation*' (DIPT) or '*deformation induced martensitic transformation*' (DIMT). The DIMT of austenitic stainless steels as well as other TRIP steels has been well documented to enhance the ductility through continuous relaxation process of an internal strain energy accumulated during inelastic deformation [16-21].

The transformation kinetics of these TRIP steels has been reported to depend on the stability of austenite phase as well as the loading mode of inelastic deformation, which is in turn directly related to their overall ductility [16, 20]. A more stable austenite phase was observed to exhibit a slower transformation rate resulting into much enhanced uniform elongation by suppressing necking via continuous martensitic transformation though entire period of inelastic deformation. Highly stable austenite was, on the other hand, observed to be ineffective for ductility enhancement due to the suppression of martensitic transformation [22,23]. Various kinetics relations for TRIP steels have been suggested to account for these transformation characteristics. The kinetics equation proposed by

*Corresponding author: ywchang@postech.ac.kr

Olson *et al*. [4,24] attempted to predict volume fraction of transformed martensite phase by relating the probability of generating martensite nuclei to the number of shear band intersections. Remy [25] has also reported a kinetics relation for transformation from austenite (γ) to ε-Ms in a Fe-0.2C-26Mn steel to prescribe volume fraction of transformed ε-Ms in terms of inelastic strain. Another interesting result was reported by Choi *et al*. [18] in relation to the formation kinetics of ε-Ms and deformation twins in Fe-25Mn-0.2C steel at various temperatures, in which both of them were treated as relaxation processes of internal strain energy accumulated during inelastic deformation as prescribed by the internal variable theory. Transformation to ε-Ms was observed up to 57 °C, while deformation twins were found to form above 127 °C in this Fe-25Mn-0.2C steel with the different nucleation rates of n=1.4 and 1.0, respectively.

High manganese steels have recently drawn much interest in steel industries in an attempt to reduce the production cost by replacing such expensive alloying elements, Ni and Cr, etc [19]. Fe-12Mn steel has been developed as one of the promising alloys to replace 9% Ni steels generally used as cryogenic structural materials. This Fe-12Mn steel containing ε-Ms has typically been observed to exhibit the deformation induced phase transformation (DIPT) from ε-Ms to α-Ms during inelastic deformation even at cryogenic temperatures. The exact mechanisms and kinetics of DIPT in this steel has not, however, been understood clearly to date. The DIPT in Fe-12Mn steel has thus been investigated in the present study, especially in relation to the transformation kinetics from ε-Ms to α-Ms during inelastic deformation together with its effect on ductility enhancement at various temperatures between 77 K and room temperature (RT). Volume fractions of transformed α-Ms were first measured by performing step-wise tensile tests at the various temperatures. These transformation results were then subsequently analyzed by the kinetics equation proposed by one of the authors based on an internal variable theory for inelastic deformation [15,20].

2. EXPERIMENTAL PROCEDURES

The materials used in this study was a Fe-12Mn steel prepared by an ingot casting after vacuum induction melting of high purity elements under an argon gas atmosphere. Very small amount of carbon was contained in this present alloy and titanium and boron were added to improve cryogenic mechanical properties of Fe-12Mn steel [26,27]. The chemical composition of the alloy is listed in Table 1. The ingot was then hot rolled at 1,373 K to reduce the initial thickness of 70 mm to 11.8 mm in 5 passes before subsequent air cooling. The specimens for tensile tests were prepared along the rolling direction directly from this hot rolled plate with the cross section area of 2 mm × 5 mm and 12.5 mm gauge length. Tensile tests were then carried out under the initial strain rate of 10^{-2} s^{-1} using an Instron 8862 model at the three different temperatures of 298 K (RT), 123 K, and 77 K to examine the temperature effects on transformation kinetics as well as mechanical properties.

Table 1. Chemical compositions of Fe-12Mn steel (wt%)

Mn	C	Al	Ti	B	N	Fe
11.98	0.001	0.032	0.015	0.002	0.0025	Bal.

In order to investigate the stability of ε-Ms and transformation kinetics to α'-Ms at low temperatures, step-wise strain tests were also performed with the same specimen as in the tensile tests at the four different temperatures. The volume fractions of each phase before and during inelastic deformation were measured by using the Rietveld method, an X-ray profile fitting technique utilizing the analysis program, 'Materials Analysis Using Diffraction' (MAUD) [28,29].

The specimens before and after tensile test were subsequently polished with diamond paste with 1 μm size before electro-etching in an etchant consisting of 10% perchloric acid ($HClO_4$) and 90% acetic acid (CH_3COOH). Microstructures were then examined by using an electron backscatter diffraction (EBSD) analysis using a field emission scanning electron microscope (FE-SEM, model XL 30S FEG) and also using a transmission electron microscope (TEM, model JEOL JEM-2100F). The transformation temperatures during a continuous cooling were also determined through a dilatometer test using a cylindrical rod specimen with the dimensions of 10 mm in length and 3 mm in diameter under the cooling rate of 1 K/s.

3. RESULTS

3.1. Microstructures

It is now well known that the two stage transformations (γ →ε→α) can take place in high manganese steels containing 10~14.5% manganese as can be observed in the Fe-Mn phase diagram given in Fig. 1 [30]. The microstructure of as-received (AR) sample can indeed be observed to contain α-Ms together with fine ε-Ms in an inverse pole figure map and a phase map of EBSD given in Figs. 2(a) and (b), respectively. Most of the ε-Ms is seen to locate around α'-Ms boundaries, while α'-Ms was typically observed in a blocky form containing twin boundaries with {112} twin planes as shown in Fig. 2(a), a somewhat different morphology from the usual martensites generally observed in the forms of lath or plate type [26,27]. These unusual microstructures might also be generated from the two stage transformations (γ→ε→α') during the cooling process after hot rolling [30,31].

Dilatation curves of Fe-12Mn steel given in Fig. 3(a) were obtained during a continuous cooling under the cooling rate of 1 K/s after heating the steel under the rate of 20 K/s. Two stage transformations (γ→ε→α') during the cooling process can clearly be observed from the magnified curve given in

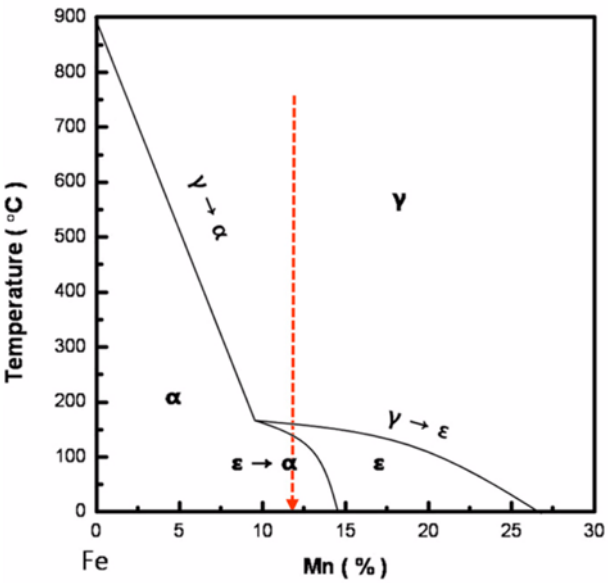

Fig. 1. Fe-Mn phase diagram exhibits two stage phase transformation of γ→ε→α' during a continuous cooling process [30].

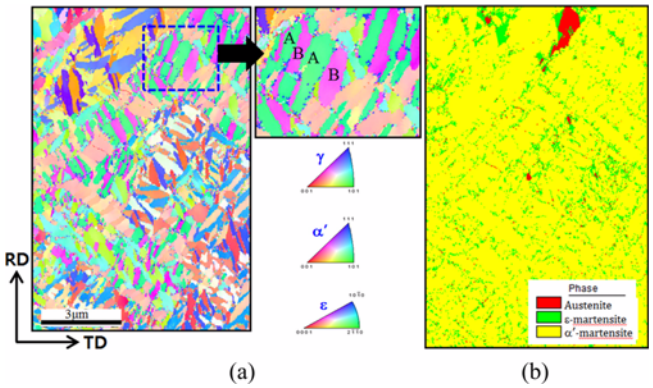

Fig. 2. EBSD maps of the present alloy; (a) inverse pole figure map and (b) phase map of AR specimen.

Fig. 3(b) and the transformation temperatures determined from the figure are listed in Table 2. This two stage transformation was, however, not observed under the faster cooling rate of 5 K/s and 10 K/s. Austenite was found to transform first to ε-Ms within a narrow temperature range from 463 K to 453 K, while ε-Ms can be observed to transform subsequently to α'-Ms below 453 K. A large volume expansion has been reported to develop during this two stage transformation, [30,32-34] which appears to be accommodated by twin boundaries containing large number of twinning dislocations between the α'-Ms as shown in a TEM micrograph given in Fig. 4.

The sequence of two stage transformation (γ→ε→α) is schematically shown in Fig. 5. During the cooling, ε-Ms phase forms first along the prior γ boundaries with about 0.7% volume contraction and then α-Ms is generated by transforming

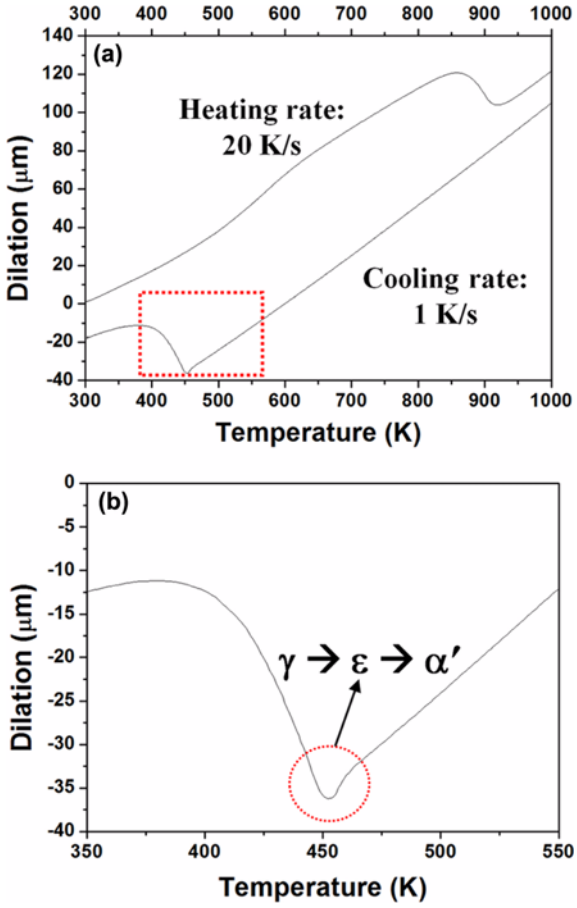

Fig. 3. (a) Dilatation curves of Fe-12Mn steel were obtained under the heating and cooling rate of 20 K/s and 1 K/s, respectively. (b) Enlarged cooling curve marked in (a) show a two stage transformation during a continuous cooling under the cooling rate of 1 K/s.

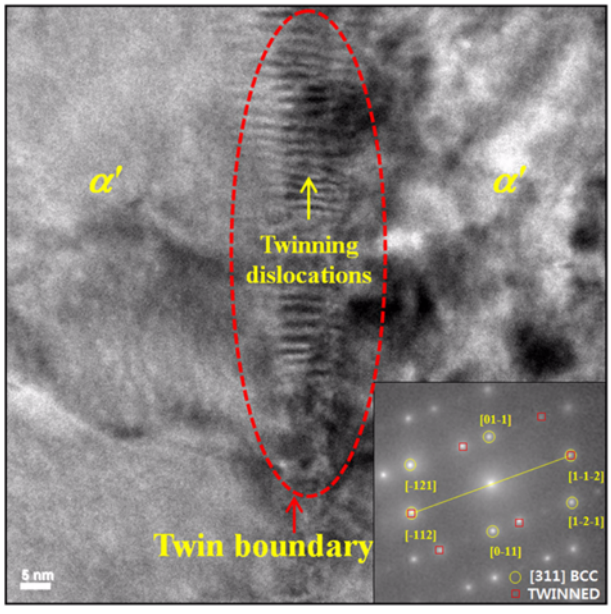

Fig. 4. TEM micrograph exhibits twin boundary formed between α'-Ms containing numerous twinning dislocations.

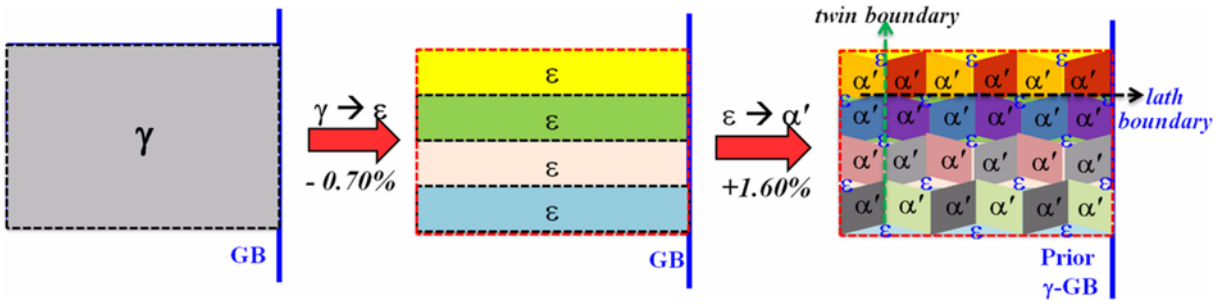

Fig. 5. Two stage transformation of (γ→ε→α) is schematically shown, exhibiting twin boundaries formed between α'-Ms to accommodate large volume expansion accompanying transformation.

Table 2. Transformation temperatures of Fe-12Mn steel obtained from dilatation curves

Heating 20 K/s	A_s^{ε}	A_f^{ε}	$A_s^{\alpha'}$	$A_f^{\alpha'}$
	170	355	475	665
Cooling 1 K/s	M_s^{ε}	M_f^{ε}	$M_s^{\alpha'}$	$M_f^{\alpha'}$
	187	183	182	85

Table 3. Tensile properties obtained at the various temperatures under the strain rate of 10^{-2}/s

Temp. (K)	YS (MPa)	UTS (MPa)	UE (%)	TE (%)
RT	309.5	1032.4	9.2	20.7
123	548.5	1395.0	12.3	22.1
77	676.5	1704.0	16.5	24.6

ε-Ms with a large volume expansion of about 1.6% upon further cooling. To accommodate this large volume expansion, twins are formed in these α-Ms laths, while leaving some untransformed ε-Ms on the lath boundaries as observed in the EBSD micrographs given in Fig. 2.

3.2. Tensile test results

Tensile stress-strain curves were obtained under the strain rate of 10^{-2} s^{-1} at the various temperatures and the results are shown in Fig. 6. These tensile curves exhibit larger elongation together with larger tensile strength as the test temperature was lowered, unlike most of the crystalline materials having larger tensile strength with much reduced elongation at lower temperatures. Various tensile properties obtained from these tensile tests are listed in Table 3 to show the maximum

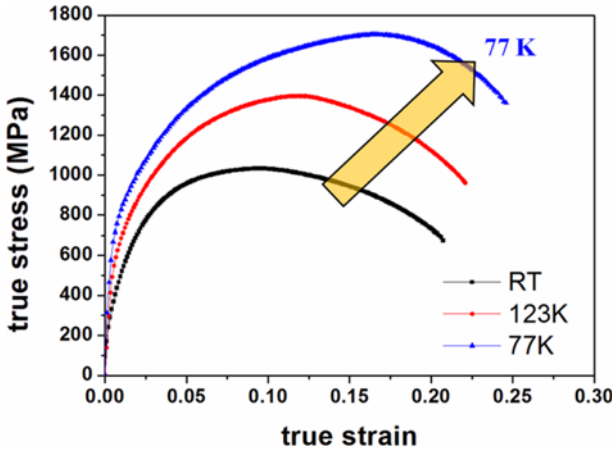

Fig. 6. Tensile stress-strain curves were obtained under the strain rate of 10^{-2}/s at the three different temperatures to exhibit larger elongation together with higher tensile strength at lower temperature.

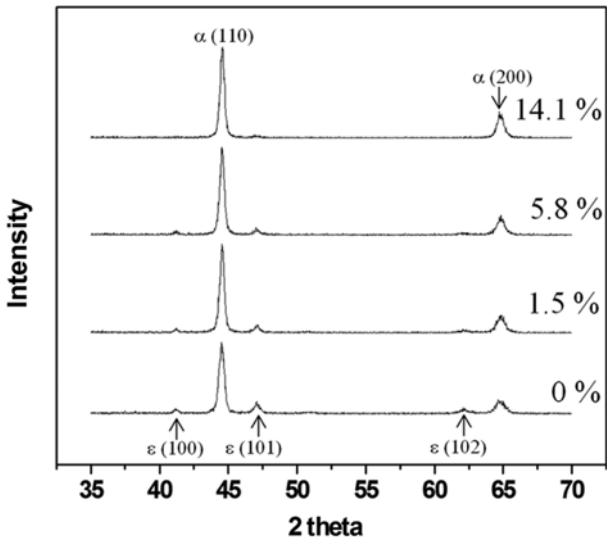

Fig. 7. X-ray diffraction patterns were obtained at the various strains during the tensile test at room temperature.

total elongation of 24.6% with the largest tensile strength of 1,704 MPa at 77 K. Progressive X-ray diffraction patterns are given in Fig. 7 to show diminishing and increasing intensities of ε-Ms and α-Ms peaks, respectively during inelastic deformation at room temperature indicating continuous phase transformation from ε-Ms to α-Ms. Deformation induced phase transformation of ε-Ms to α-Ms was also observed during a step-wise tensile test even at the lowest temperature of 77 K as shown in Fig. 8(a). The observed enhancement of ductility at lower temperatures can thus be accounted for by the DIPT from ε-Ms to α-Ms, as was reported previously for other TRIP steels where elongation was strongly related with the transformation rate [16-20].

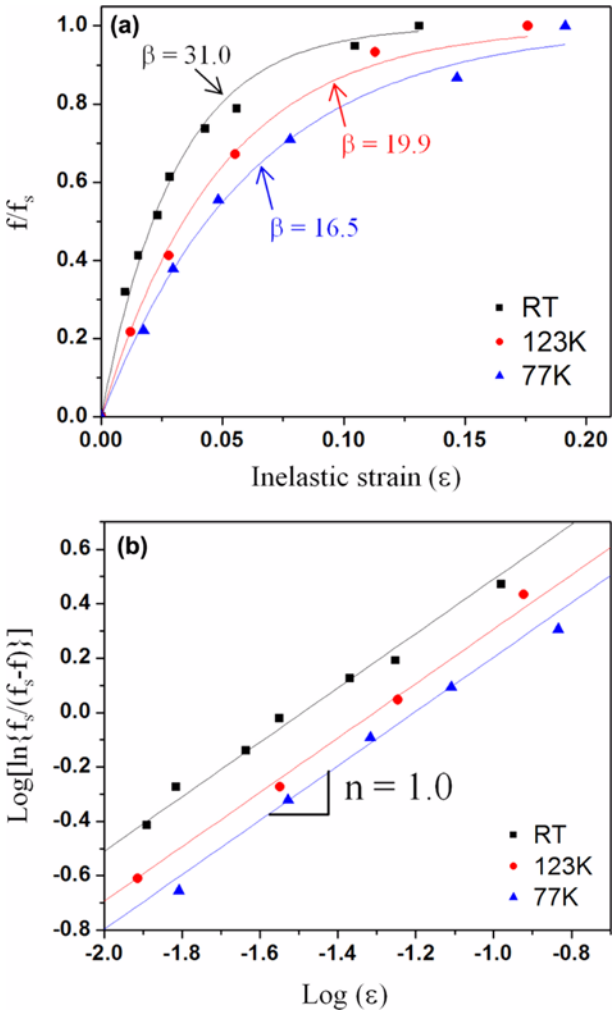

Fig. 8. (a) Transformation curves show the variations of volume fraction of α′-Ms during the tensile tests. (b) Double log scale plots of $\mathbf{f}_\alpha$ vs. inelastic strain, ε provide the slope of **n** = 1.0.

3.3. Transformation rate

The transformation of ε→α' were analyzed in the present study using the kinetics relation proposed by one of the authors as, [16]

$$\left(\frac{\mathbf{f}}{\mathbf{f_s}}\right) = 1-\exp(-\beta\varepsilon^{\mathbf{n}}) \qquad (1)$$

with the parameters **f** and $\mathbf{f}_s$ denoting the volume fraction and its saturation value of transformed phase. The parameter β and **n** in Eq. (1) characterizes respectively the stability of parent phase and the formation rate of nucleation sites defined as,

$$\mathbf{n} = \left(\frac{\mathbf{d\ ln\ N^I}}{\mathbf{d\ ln\ \varepsilon}}\right) \qquad (2)$$

where N^I is the number of nucleation sites formed during inelastic deformation [16]. This nucleation rate parameter **n** could also be regarded as a deformation mode parameter, since it depends on the loading mode and stress state. This kinetics relation given in Eq. (1) has successfully been demonstrated as one of the most effective kinetics relation for the various DIMT behaviors [16-20].

A non-linear least square fitting method was subsequently used for the transformation data given in Fig. 8(a) using Eq. (1) to determine the three kinetics parameters **n**, $\mathbf{f}_s$, and β and the results are listed in Table 4 together with the initial volume fraction ($\mathbf{f}_o$) of ε-Ms. The values of n were in fact obtained from the curve fitting as very close to 1.0. To clarify further, this deformation mode parameter (**n**) was also estimated as the slope of the double log relation of Eq. (1) given as,

$$\mathbf{Log}\left\{\mathbf{ln}\left[\frac{\mathbf{f_s}}{(\mathbf{f_s}-\mathbf{f})}\right]\right\} = \mathbf{Log}\ \beta + \mathbf{n}\ \mathbf{Log}\ \varepsilon \qquad (3)$$

The slope in Fig. 8(b) was indeed obtained as **n** = 1.0, providing the same value obtained previously for a multiphase Fe-C-Si-Mn TRIP steel [16]. The solid lines given in Fig 8(a) are in fact predicted transformation curves using the values given in Table 4 in Eq. (1). Different deformation and transformation behavior have been reported for austenitic stainless steels with **n** = 2.2 [17, 20]. Above result then implies that the formation characteristic of nucleation sites in Fe-12Mn steel is similar to that in multiphase TRIP steels.

Deformation induced martensitic transformation (DIMT) of austenite (γ) observed in general TRIP steel has been reported previously and schematic free energy relation is shown in Fig. 9. Austenite start to transform to α'-Ms at the M_s temperature, at which the critical driving force $\Delta\mathbf{G}^*$ is reached by sufficient undercooling to overcome non-chemical energy barriers such as interfacial and elastic energy [3,4,17]. Transformation of γ phase to martensite is now well observed to occur above the M_s, but below the M_d temperature during plastic deformation. It has been proposed previously that internal strain energy (Δu^I) accumulated during plastic deformation can effectively provide required additional driving force for deformation induced martensitic transformation (DIMT) of γ phase as schematically illustrated in Fig. 9 [17]. The value of stability parameter β was observed to decrease in these steels with reduced transformation rate at higher test temperature, since austenite phase becomes more stable at higher temperatures requiring more internal strain energy at higher temperatures [17-20].

Table 4. Values of the kinetics parameters, n, f_s, and β determined from the transformation data using Eq. (1) together with the initial volume fraction (f_o) of ε-martensite

Temperature (K)	298	123	77
n	1.0	1.0	1.0
f_o (%)	19.6	18.5	23.1
f_s (%)	19.4	18.3	22.7
β	31.0	19.9	16.5

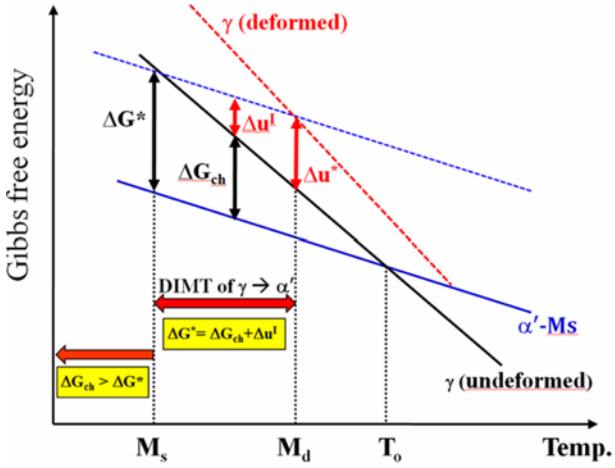

Fig. 9. Deformation induced martensitic transformation (DIMT) of γ →α'-Ms is shown to take place even above the M_s temperature with the aid of internal strain energy Δu^I in general TRIP steels [20]. A critical internal strain energy Δu^* is required for the DIMT below the M_d temperature, but above the M_s temperature.

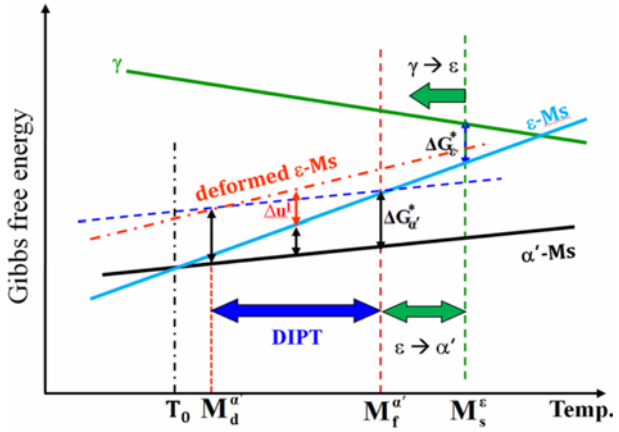

Fig. 10. Schematic free energy diagram constructed for deformation induced phase transformation (DIPT) of ε-Ms→α'-Ms in a Fe-12 Mn steel based on the present study.

The stability parameter β in the present Fe-12Mn steel is, however, found to show a reversed trend of temperature dependence with the reduced value of β = 16.5 at 77 K (–196 °C) from β = 31.0 at RT. Contrary to the case of austenite phase being more stable at higher temperatures, ε-Ms became more stable at lower temperature to transform ε-Ms more slowly during the inelastic deformation at lower temperature as evidenced by Fig. 8. Furthermore, saturation values ($\mathbf{f_s}$) of α'-Ms were found to become close to those of the initial volume fraction ($\mathbf{f_o}$) of ε-Ms at each test temperature to imply that almost all the ε-Ms transformed into α'-Ms. This slower transformation rate appears to play a critical role on enhancing tensile ductility at lower temperature via continuous relaxation of internal strain energy used as an additional driving force for the DIPT, as was suggested by the internal variable theory [15,16].

4. DISCUSSIONS

In the present Fe-12Mn alloy, austenite was observed to transform first to ε-Ms and then to α'-Ms during the cooling with the chemical driving force $\Delta \mathbf{G_{ch}}$, solely due to the difference in Gibbs free energies between the two phases. This is therefore a thermal energy generated by undercooling from $\mathbf{M_s}^{\varepsilon}$ to $\mathbf{M_f}^{\alpha'}$ temperature as schematically illustrated in Fig. 5. The ε-Ms cannot, however, transform to α'-Ms below $\mathbf{M_f}^{\alpha'}$ temperature, since the chemical driving force is not sufficient for transformation into α'-Ms. Internal strain energy accumulated during plastic deformation can naturally provide an additional driving force for the transformation of ε-Ms to α'-Ms as schematically described in Fig. 10, which was constructed based on the observation from the present study. It can be seen from this free energy diagram, more internal strain energy is required at lower temperature due to the reduction of chemical driving force ($\Delta \mathbf{G_{ch}}$), resulting into slower transformation rate at lower temperature to provide the largest elongation at the liquid nitrogen temperature (LNT) for the present Fe-12 Mn alloy. The finishing temperature $\mathbf{M_d}$ of DIPT appears to be below the LNT for the present alloy, although it was not determined experimentally in the present study. This free energy relation between the ε-Ms and α'-Ms phases is thought to provide a plausible description for deformation induced phase transformation (DIPT) together with the ductility enhancement mechanism at lower temperatures. This type of stability-temperature relationship has also been reported previously by providing a schematic free energy diagram of γ, ε-Ms, and α'-Ms in stainless steels [35]. Difference in Gibbs free energy between ε-Ms and α'-Ms is shown to decrease continuously with decreasing temperature and ε-Ms becomes more stable than α'-Ms below T = ~370 K in stainless steels, a similar trend observed in the present alloy.

Internal strain energy accumulated during the plastic deformation can effectively be relaxed through the DIPT/DIMT leading into ductility enhancement as well as strengthening by the harder transformed phase. The degree of ductility enhancement appears to depend directly on the stability of transforming phase characterized by the stability parameter β, which was found to become larger at lower temperature to provide much slower transformation rate resulting into larger elongation in the present Fe-12Mn steel.

5. CONCLUSIONS

Large ductility enhancement at lower temperatures in Fe-12Mn steel has been studied based on an internal variable theory for inelastic deformation to obtain the following results.

(1) Deformation induced phase transformation (DIPT) of ε-Ms→α'-Ms could successfully be prescribed by the kinet-

ics relation given by Eq. (1), proposed based on an internal variable theory for inelastic deformation.

(2) The ε-Ms was found to become more stable as temperature was reduced, which was characterized by the lower value of $\beta = 16.5$ at 77 K from $\beta = 31.0$ at RT, contrary to the case DIMT of austenite. The higher elongation at LNT could be accounted for by the slower transformation rate in Fe-12Mn steel.

(3) Deformation mode parameter **n** was found to be **n** = 1.0, which is the same value observed in multi-phase TRIP steels.

(4) The DIPT of ε-Ms→α'-Ms appears to occurs above the T_o temperature, in contrast to the DIMT of γ→α' observed below the T_o temperature in various TRIP steels.

ACKNOWLEDGMENTS

This study has been carried out with the research funds provided by POSCO, for which the authors are grateful.

REFERENCES

1. T. Angel, *J. Iron and Steel Inst.* **177**, 165 (1954).
2. D. C. Ludwigson and J. A. Berger, *J. Iron and Steel Inst.* **207**, 63 (1969).
3. I. Tamura, T. Maki, and H. Hato, *Trans. Iron and Steel Inst*. Japan **10**, 163 (1970).
4. G. B. Olson and M. Azrin, *Met. Trans. A* **9**, 713 (1978).
5. L. Remy and A. Pineau, *Mater. Sci. Eng.* **26**, 123 (1976).
6. Y. S. Chung, Y. K. Lee, D. K. Matlock and M.C. Mataya, *Met. Mater. Int.* **17**, 553 (2011).
7. J. M. Jang, S. J. Kim, N. H. Kang, K. M. Cho, and D. W. Suh, *Met. Mater. Int.* **15**, 909 (2009).
8. K. H. Kwon, J. S. Jeong, J. K. Choi, Y. M. Koo, Y. Tomota, and N. J. Kim, *Met. Mater. Int.* **18**, 751 (2012).
9. V. F. Zackay, E. R. Parker, D. Fahr, and R. Busch, *Trans. Am. Soc. Met.* **60**, 252 (1967).
10. O. Matsumura, Y. Sakuma, and H. Takechi, *Trans. Iron and Steel Inst.* **27**, 570 (1987).
11. O. Matsumura, Y. Sakuma, and H. Takechi, *Scripta Mater.* **21**, 1301 (1987).
12. H. C. Chen, H. Era, and M. Shimizu, *Met. Trans. A* **20**, 437 (1987).
13. Y. Sakuma, O. Matsumura, and H. Takechi, *Met. Trans. A* **22**, 489 (1991).
14. Y. Sakuma, D. K. Matlock, and G. Krauss, *J. Heat Treat.* **9**, 109 (1990).
15. T. K. Ha and Y. W. Chang, *Acta Mater.* **46**, 2741 (1998).
16. J. H. Chung and Y. W. Chang, *Tetsu-to-Hagane* **79**, 665 (1993).
17. H. C. Shin, T. K. Ha, and Y. W. Chang, *Scripta Mater.* **45**, 823 (2001).
18. H. C. Choi, T. K. Ha, H. C. Shin, and Y. W. Chang, *Scripta Mater.* **40**, 1171 (1999).
19. C. Y. Lee, T. K. Ha, and Y. W. Chang, *J. Kor. Inst. Met.* **39**, 1347 (2001).
20. J. H. Chung, J. B. Jeon and Y. W. Chang, *Met. Mater. Int.* **16**, 533 (2010).
21. M. G. Lee and S. J. Kim, *Met. Mater. Int.* **18**, 425 (2012).
22. C. G. Lee, S. J. Kim, B. H. Song, and S. H. Lee, *Met. Mater. Int.* **8**, 435 (2002).
23. C. Jing, D. W. Suh, C. S. Oh, Z. Wang, and S. J. Kim, *Met. Mater. Int.* **13**, 13 (2007).
24. G. B. Olson and M. Cohen, *Metall. Trans. A* **6**, 791 (1975).
25. L. Remy, *Metall. Trans. A* **8**, 253 (1977).
26. S. K. Hwang and J. W. Morris, *Metall. Trans. A* **10**, 545 (1979).
27. S. K. Hwang and J. W. Morris, *Metall. Trans. A* **11**, 1197 (1980).
28. H. M. Rietveld, *J. Appl. Cryst.* **2**, 65 (1969).
29. R. J. Hill and C. J. Howard, *J. Appl. Cryst.* **20**, 467 (1987).
30. Z. Nishiyama, *Martensitic Transformation*, p.53, Academic Press (1978).
31. K. Shimizu and Y. Tanaka, *Trans. Jpn. Inst. Met.* **19**, 685 (1978).
32. K. K. Jee, S. H. Baik, B. J. Lee, M. C. Shin, and C. S. Choi, *Scripta Mater.* **33**, 1901 (1995).
33. Y. Lü, B. Hutchinson, D. A. Molodov, and G. Gottstein, *Acta Mater.* **58**, 3079 (2010).
34. C. Y. Kang and T. Y. Hur, *Korean J. Met. Mater.* **50**, 413 (2012).
35. K. Datta, J. Post, and A. Dinsdale, *Acta Mater.* **57**, 3321 (2009).